Three types of computer-generated hologram synthesized from multiple angular viewpoints of a three-dimensional scene

David Abookasis and Joseph Rosen

We describe various techniques to synthesize three types of computer-generated hologram (CGH): the Fresnel–Fourier CGH, the Fresnel CGH, and the image CGH. These holograms are synthesized by fusing multiple perspective views of a computer-generated scene. An initial hologram is generated in the computer as a Fourier hologram. Then it can be converted to either a Fresnel or an image hologram by computing the desired wave propagation and imitating an interference process of optical holography. By illuminating the CGH, a 3D image of the objects is constructed. Computer simulations and experimental results underline the performance of the suggested techniques.

OCIS codes: 090.1760, 090.2870, 070.2580, 070.4560, 100.6890.

1. Introduction

Synthesizing a computer-generated hologram (CGH) of a 3D object is a heavy computational task.[1] We need to superpose the mathematical contributions of many waves originating from many points on the objects, when obviously not all of them are located at the same distance from the hologram plane. Recently, we developed a new procedure for generating a CGH of general 3D objects by fusing multiple angular projections of computer-designed objects.[2] By a specific computing process of data reduction on all angular perspectives of the 3D object, a single 2D complex function is obtained representing the wavefront distribution on the hologram plane. This complex function is then conventionally encoded in a CGH with real and positive transparency values. Illuminating the CGH by a plane wave constructs an image of the original object with the desired 3D cues. This method reduces the computation load to that of CGHs of 2D objects, and more importantly, it enables us to synthesize a hologram of both realistic[3] and computer-generated[2,4] 3D objects. Thus in some cases this technique can replace the complicated interferometric process of hologram recording. Furthermore, we have shown[2,3] that merging angular projections together yields a Fourier hologram equivalent to the well-known optical Fourier hologram[5] recorded by a coherent light source. As discussed in Ref. 2, although the input data in our method are a set of the object's angular viewpoints, our technique differs from computing CGHs by stereoscopic technique[6] or by multiplexing[7] CGHs. In this study, the procedure of computing a CGH is extended to create other types of hologram.

There are three well-known types of hologram: the Fourier hologram, the Fresnel hologram, and the image hologram.[8] The differences among these holograms can be manifested by different optical setups placed between the object and the hologram planes as described below.

In a Fourier hologram, the recording plane resides in a plane that will yield the Fourier transform of the object interfering with a reference wave. Reconstruction of the 3D object from the Fourier hologram can be simulated with a computer by applying the fast-Fourier transform numerical tool. Optical reconstruction can be achieved using a Fourier lens and illuminating the hologram with a plane wave. The Fresnel hologram is generated from an object located within a Fresnel region in which the Fresnel diffraction formula is satisfactorily valid.[9] In principle, the space between the Fresnel hologram and the viewer is free of any lens or other optical device. This feature makes the Fresnel hologram more practical as a

The authors are with the Department of Electrical and Computer Engineering, Ben-Gurion University of the Negev, P.O. Box 653, Beer-Sheva 84105, Israel. J. Rosen's e-mail address is rosen@ee.bgu.ac.il.

Received 24 January 2006; revised 7 April 2006; accepted 7 April 2006; posted 11 April 2006 (Doc. ID 67374).

0003-6935/06/256533-06$15.00/0

holographic display than the Fourier hologram. The generation of the Fresnel CGH of computer-generated objects from a series of projections using the principle of computer tomography, was proposed by Sando *et al.*[4] In the present study, we extend this work, suggest two types of Fresnel CGH, and discuss their advantages and limitations.

In the case of an image hologram, the hologram is recorded by imaging an object on the plane of the holographic recording medium and interfered with a tilted reference wave. The constructed 3D image appears to float at the hologram plane, where parts of the image are extended outside the hologram and other parts remain inside the hologram. This feature makes them highly attractive as a 3D display for hardcopy and video applications. The generation of the image CGH of 3D objects has been proposed by Leseberg.[10] Our image CGH is formed in two steps. First, the 3D image is digitally created from the Fourier hologram. Then, equivalent to the optical interference process, the image is constructed by superposing a digital reference wave. Contrary to other methods, ours has less computation complexity, and it can be applied for real existing objects.

The paper is organized as follows: Section 2 briefly describes the Fourier CGH algorithm generation for 3D objects through a set of scene projections. Sections 3–5 discuss the generation of three types of CGH and present numerical and experimental results for each. The paper ends with a conclusion in Section 6.

2. Synthesizing Fourier Computer-Generated Holograms Using Multiple Points of View

In this section, we briefly summarize the algorithm for synthesizing Fourier CGH from multiple perspectives, first presented in Ref. 2, and shown schematically in Fig. 1.

The first step is to generate a 3D object in the computer's memory. Next, the set of the object's angular projections is computed. Then, each projection is multiplied by a corresponding phase function, and the product is summed to a single complex value. The end product of this process is a single 2D complex function representing the wavefront distribution on the hologram plane. Every complex value of this function is computed from a different angular projection and is positioned at the wavefront matrix precisely in the scanning order. The mathematical expression of the m, nth complex value at the wavefront matrix is given by

$$s(m,\ n) = \int\int p_{mn}(x_p,\ y_p) \times \exp[-i2\pi b(x_p \sin \varphi_m + y_p \sin \theta_n)] \times \mathrm{d}x_p \mathrm{d}y_p, \quad (1)$$

where $p_{mn}(x_p, y_p)$ is the m, nth perspective image viewed from the angles (φ_m, θ_n) in the horizontal and vertical directions, respectively; (x_p, y_p) are the coordinates of each projection; and b is a real-valued constant determining the hologram scale. Finally,

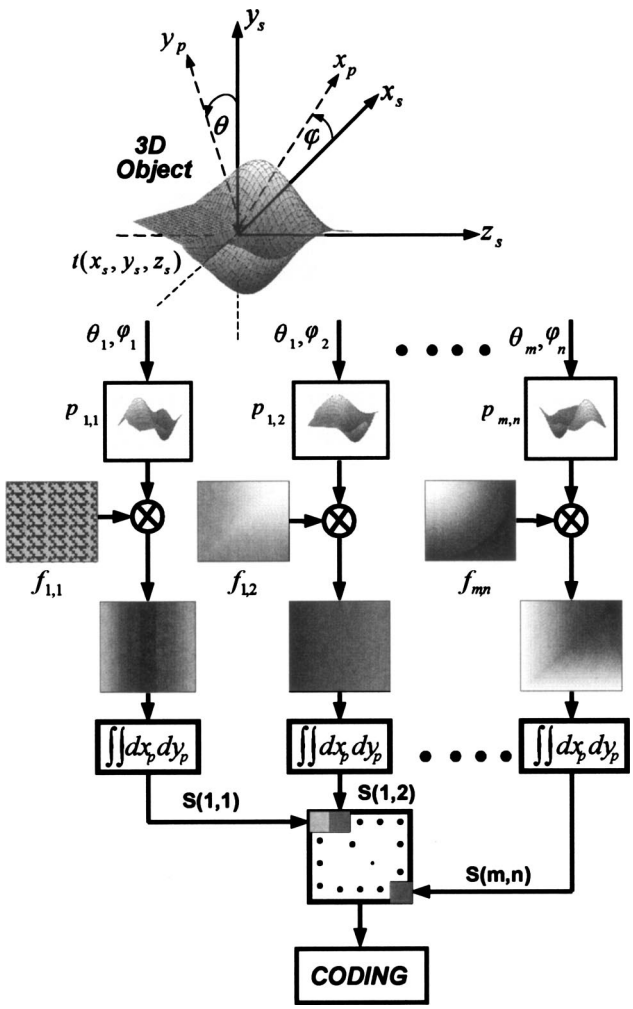

Fig. 1. CGH algorithm. $f_{m,n} = \exp[-i2\pi b(x_p \sin \varphi_m + y_p \sin \theta_n)]$.

the complex matrix $s(m, n)$ is coded to a real- and positive-valued matrix to be used as a holographic transparency. The complete computational process is illustrated schematically in Fig. 1.

We have shown in Ref. 2 that this algorithm generates a single complex function $s(m, n)$ equal to the wavefront on the Fourier plane sampled at the m, n points. Therefore for large values of m and n, the resulting CGH is equivalent to an optical Fourier hologram of a realistic 3D scene recorded by a coherently illuminated system. Based on the Fourier hologram, we now propose new types of CGH.

3. Fresnel–Fourier Computer-Generated Hologram

A. Algorithm

The weaknesses of the Fourier hologram are the lack of a virtual image and the need to place a lens between the viewer and the hologram to observe the constructed image. To overcome these limitations, we encode the transmission function of the Fourier lens into the hologram. We call this type of hologram a Fresnel–Fourier CGH, because on the one hand the real and virtual images are constructed at a Fresnel distance from both sides of the hologram, and on the

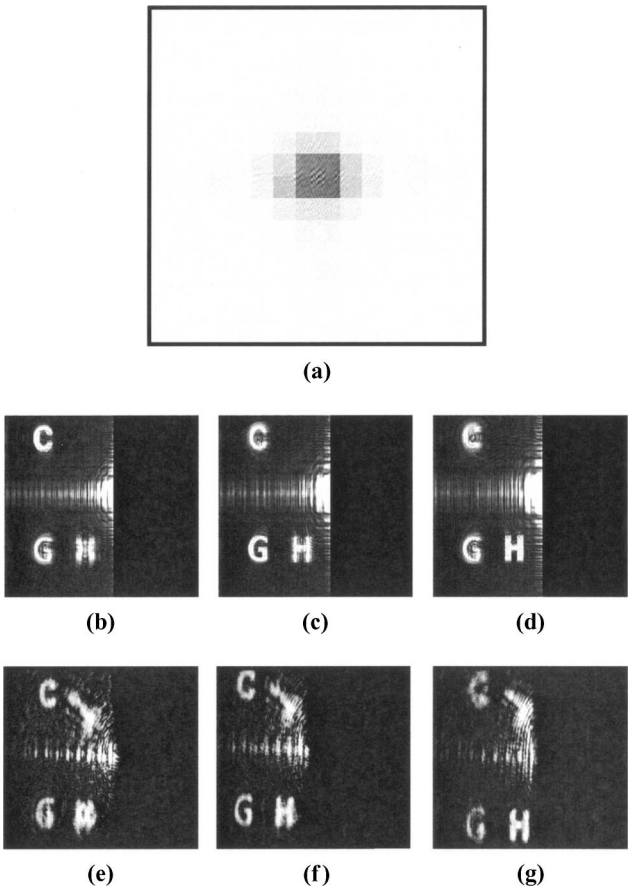

Fig. 2. (a) Enlarged portion (300 × 300 pixels of 601 × 601) of the color-inverted Fresnel–Fourier CGH. (b)–(d) Digital reconstruction images from the hologram appear in (a), along the optical axis. (e)–(g) The optical reconstruction in the vicinity of the back of an imaging lens for three transverse planes at 470, 510, and 550 mm for the C, G, and H planes, respectively. We used the imaging lens to bring the far reconstruction plane nearer and for better visualization.

other, this hologram is derived directly from a Fourier hologram in the sense that it is actually a product of two elements, the Fourier hologram and a lens, which are attached. In addition, as Fig. 2(a) shows, the spatial information is distributed all over the hologram in a way similar to a Fourier hologram without any local relation to the shape of the objects.

As mentioned earlier, our algorithm generates a single complex function $s(m, n)$ from the entire projection. This complex function in continuous coordinates (u, v) is related to the 3D object function $t(x_s, y_s, z_s)$ by the following relation:

$$s(u, v) \propto \iiint t(x_s, y_s, z_s) \times \exp\{-i2\pi\alpha[ux_s + vy_s + \sigma z_s(u^2 + v^2)]\} \times dx_s dy_s dz_s, \quad (2)$$

where α, σ are some constants that enable us to control the transverse and longitudinal scales separately, and (x_s, y_s, z_s) are the coordinates of the object space. The mathematical steps yielding Eq. (2) from Eq. (1) are extensively detailed in Ref. 2. Equation (2) actually describes the wavefront distribution on the back focal plane obtained from a coherently illuminated 3D object $t(x_s, y_s, z_s)$ positioned in the vicinity of the front focal point. The function $s(u, v)$ is equivalent to a Fourier hologram recorded by a coherently illuminated system and with a 3D object as the system's input. Therefore to obtain the Fresnel–Fourier hologram, the complex function $s(u, v)$ is multiplied by a quadratic phase function representing the lens transfer function. To overcome the twin image effect, $s(u, v)$ is also multiplied by a linear phase function representing the off-axis reference wave. Then, the Fresnel–Fourier hologram transmission is given by

$$H_{FF}(u, v) = \Re\left\{s(u, v)\exp\left(\frac{-i\pi r^2}{\lambda z_{\Im}}\right) \times \exp\left(\frac{i2\pi \sin\psi}{\lambda} v\right)\right\} + c, \quad (3)$$

where $\Re$ represents the real operator, $r^2 = u^2 + v^2$, ψ is the inclination angle of the first diffraction order, and c is a constant bias added to avoid negative values in the hologram's transmission. The image is constructed at a distance $z_{\Im}$ from the hologram. To calculate $z_{\Im}$ from the parameters of the actual experiment, we look on the location of the focal point obtained from a quadratic phase function displayed on the hologram plane. The transmission of a quadratic plus linear phase function, with γ concentric cycles from the center to the perimeter, and β linear cycles is

$$H_{FF}'(u, v) = \Re\left\{\exp\left[-i8\pi\gamma\left(\frac{r}{dN}\right)^2 + i4\pi\beta\frac{v}{dN}\right]\right\}, \quad (4)$$

where N is the number of hologram pixels and d is the gap between every two successive pixels. By comparing the arguments of the quadratic phase, Eqs. (3) and (4) yield the following values for the distance between the hologram and the constructed object:

$$Z_{\Im} = \frac{(dN)^2}{8\lambda\gamma}, \quad (5)$$

and for the inclination angle of the first diffraction order:

$$\sin\psi = \frac{2\lambda\beta}{dN}. \quad (6)$$

The maximum number of cycles, γ_{max}, limits the minimal distance between the hologram and the reconstructed image. γ_{max} is calculated by assuming that the possible minimal length of the shortest cycle is of length $2d$ of two full pixels. This assumption can be formulated by the following inequality:

$$\left[2\pi\gamma\left(\frac{2r}{dN}\right)^2+2\pi\beta\,\frac{2v}{dN}\right]_{v,r=dN/2}-\left[2\pi\gamma\left(\frac{2r}{dN}\right)^2+2\pi\beta\,\frac{2v}{dN}\right]_{v,r=(dN/2)-2d}\le 2\pi. \quad (7)$$

This inequality expresses the condition that the length of the last two pixels is equal to or less than the 2 π cycle. Substituting Eqs. (5) and (6) and the approximation $\sin\psi \approx u/z_{\Im}$ into inequality Eq. (7) yields a conditional space in the shape of a cone in which the reconstructed image can be obtained. The cone has a height parallel to the z axis and an apex on the z axis at a distance $z_{\Im,\min}$ from the hologram. The distance between the hologram and the reconstructed image satisfies the following inequality:

$$z_{\Im} \ge \frac{d}{\lambda}\,(Nd+2r_o), \quad (8)$$

where r_o is the transverse radial variable of the reconstruction space. This means that the reconstructed image cannot be obtained at a distance less than $z_{\Im,\min}=d^2N/\lambda$ from the hologram, and therefore, the maximal diffraction angle is $\psi_{\max}=\tan^{-1}(\lambda/2d)$. For the present study with $\lambda = 632.8$ nm, $N = 600$, and $d = 18$ μm, the minimal allowed reconstruction distance ($r_o = 0$) from the hologram plane is $z_{\Im,\min}\approx 31$ cm, and the maximum diffracted angle is $\psi \approx 1°$.

B. Computer Simulation and Optical Experiment

The Fresnel–Fourier hologram was synthesized according to the analysis of Subsection 3.A. A 3D object composed of three planes carrying the letters C, G, and H, one on each plane at different transverse planes, was generated in the computer. The first plane with the letter C is located at the back of the scene at point $(x, y, z) = (-60, 180, -240)$ pixels, the second plane with the letter G is located at the front of the scene at point $(x, y, z) = (-60, -180, 0)$ pixels, and the third plane with the letter H was shifted to the right of the G plane at the point $(x, y, z) = (60, -180, 240)$ pixels. Each plane has an area of 100×100 pixels. In the entire experiments of this study, the 3D object was observed from an incrementally changed angle in the azimuthally and elevation angles of ±10°, where the angular displacement between every two successive projections was 0.01° in both directions. The inverted gray-scale Fresnel–Fourier hologram computed according to Eq. (3) is shown in Fig. 2(a). The images constructed from the hologram by computer simulation in three transverse planes are depicted in Figs. 2(b)–2(d). The reconstruction results were obtained by calculating the diffraction patterns from the hologram plane along the propagation axis at three different transverse planes.

To optically reconstruct the 3D object, we illuminate the computed Fresnel–Fourier CGH, which is displayed on a spatial light modulator (SLM) (CRL, Model XGA3), with a collimated beam emerging from a He–Ne laser radiating at 632.8 nm. The entire reconstruction pictures were captured with an 8-bit 795×596 pixel CCD camera (Sony-XC75CE). The three letters, C, G, and H, shown in Figs. 2(e)–2(g), appeared, respectively, at 470, 510, and 550 mm from an imaging lens ($f = 400$ mm). This imaging lens was used for clear visualization. The distance between the lens and the SLM was 160 mm. Although the experimental results without using the imaging lens have not been presented here, the reconstruction plane was observed at approximately 300 cm from the SLM. This distance satisfies the condition given in Eq. (8).

4. Fresnel Computer-Generated Holograms

A. Algorithm

In the Fresnel–Fourier hologram just described, the information is distributed globally all over the hologram, which makes it suitable for relatively long distances between the hologram and the reconstructed image. For shorter hologram–image distances, we propose a generating method of a Fresnel hologram by imitating the optical holography recording. First, the objects are digitally constructed from $s(u, v)$ by a 2D Fourier transform. Then the propagation along a distance z_F is computed by convolving the object's central transverse slice with a quadratic phase function according to the rule of Fresnel propagation in free space.[9] In the last step, we multiply the convolution operation by a linear phase to obtain the off-axis object's construction. This step also avoids the twin-image problem. The complete formula for the Fresnel CGH is

$$H_{\mathrm{Fr}}(x, y)=\Re\left\{\Im^{-1}\{s(u, v)\} * \exp\left[\frac{i\pi}{\lambda z_F}\left(x^2+y^2\right)\right]\times\exp\left(i2\pi\,\frac{\sin\psi}{\lambda}\,y\right)\right\}+c, \quad (9)$$

where $\Im^{-1}$ and the asterisk indicate the inverse Fourier transform and the convolution operator, respectively. In practice, we can convolve the digital matrix with a quadratic phase of the form $\Phi(k, l) = \exp\{i2\pi\gamma'[(2k/N)^2 + (2l/N)^2]\}$, where γ' is the number of cycles from the center to the perimeter. Calculation of the construction distance z_F versus the parameters of the experiment is similar to that in Eq. (7), but this time the diameter of the quadratic phase is less than the diameter of the SLM, depending on the chosen parameter γ'. Since the maximal diffraction angle is still $\psi_{\max}=\tan^{-1}(\lambda/2d)$, and since it is also the ratio between the hologram radius ($dN/2$) and the minimal axial distance $(dN)^2/8\lambda\gamma_{\mathrm{mx}}'$, the maximal number of cycles is $\gamma_{\mathrm{mx}}' = N/8$. Substituting γ_{mx}' into Eq. (5) indicates that the axial distance between the hologram and the constructed image satisfies the condition

$$z_F \ge \frac{d^2N}{\lambda}. \quad (10)$$

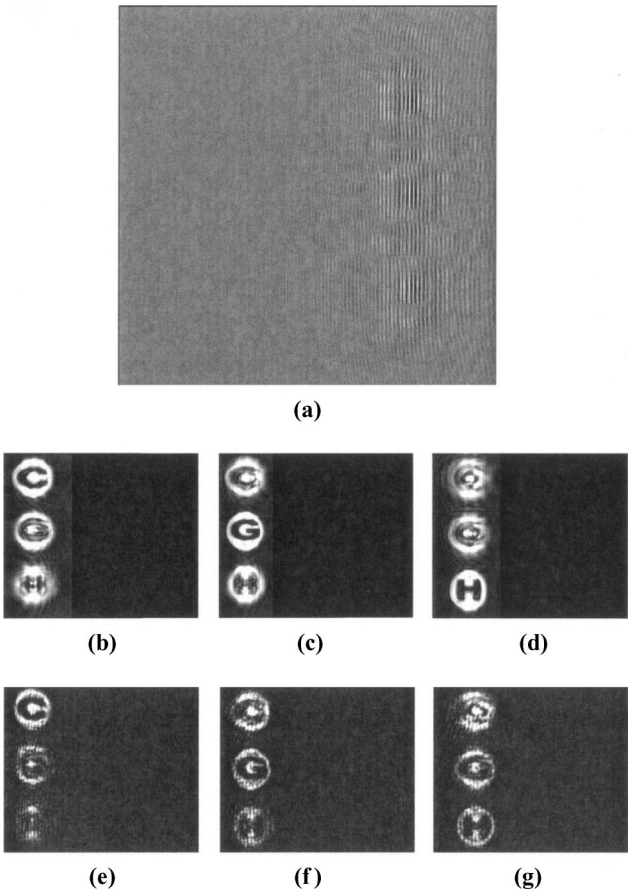

Fig. 3. (a) Enlarged portion of the Fresnel CGH. (b)–(d) Digitally reconstructed images for three successive transverse planes along the optical axis. (e)–(g) The optical reconstruction for three transverse planes at 145, 160, and 177 mm from the SLM for the C, G, and H balls, respectively.

This limit is the same as the value obtained from solving Eq. (7). Therefore in a same SLM used for the Fourier–Fresnel hologram, illuminated by the same wavelength, we have to reduce the number of used pixels on the SLM if smaller axial distances are required.

B. Computer Simulation and Optical Experiment

For the Fresnel CGH, the test object is composed of three balls with radii of 70 pixels each. Each ball is denoted by the letters C, G, H and is positioned at different depths. The C ball was located at point $(x, y, z) = (0, 220, 220)$ pixels, the G ball was located at point $(x, y, z) = (0, 0, 0)$ pixels, and finally the H ball was located at point $(x, y, z) = (0, -220, -220)$ pixels. The hologram pattern, created according to Eq. (9), and the digital reconstruction from this CGH are shown in Figs. 3(a) and 3(b)–3(d), respectively.

To optically reconstruct the 3D object, the same setup as in Fig. 3(b) was used. In Figs. 3(e)–3(g), the experimental reconstruction from the Fresnel CGH was observed at 145, 160, and 177 mm away from the SLM for C, G, and H balls, respectively. The expected image reconstruction of the C, G, and H balls should be 148.5, 160.5, and 171.7 mm. Because it is hard to precisely measure the exact location of each in-focus plane, the experimental results shown in Figs. 3(e)–3(g) fairly agree with these calculations. The experimental reconstruction from the Fresnel CGH was observed without using any lens between the hologram and the images. These results, together with those in Subsection 3.B, show that at each transverse plane a different letter of a different ball is in focus, thus indicating the success of the 3D reconstruction.

5. Image Computer-Generated Hologram

A. Algorithm

The last type of CGH considered in this study is the image hologram. After computing the inverse Fourier transform of $s(u, v)$, the image of the object's volume is constructed in the computer. Then a reference wave is added to the reconstruction volume. Consequently the distribution of the image CGH becomes

$$H_I(x, y) = \Re\left\{\Im^{-1}\{s(u, v)\}\exp\left(i2\pi \frac{\sin \psi}{\lambda} y\right)\right\} + c. \tag{11}$$

$H_I(x, y)$ given by Eq. (11) is a computed transmittance pattern, which is later displayed on the holographic display.

B. Computer Simulation and Optical Experiment

The 3D object used for demonstrating the image hologram was composed of three cubes with the letters B, G, and U. The B, G, and U cubes were positioned, respectively, at the front of the scene at point $(x, y, z) = (0, 180, 220)$ pixels, at the center of the scene at point $(x, y, z) = (0, 0, 0)$ pixels, and at the back of the scene at point $(x, y, z) = (0, -180, -220)$ pixels, respectively. The size of each cube was $120 \times 120 \times 120$ pixels. Nine projections, the central and the eight most extreme, out of 201×201 projections are shown in Fig. 4. As mentioned in Subsec-

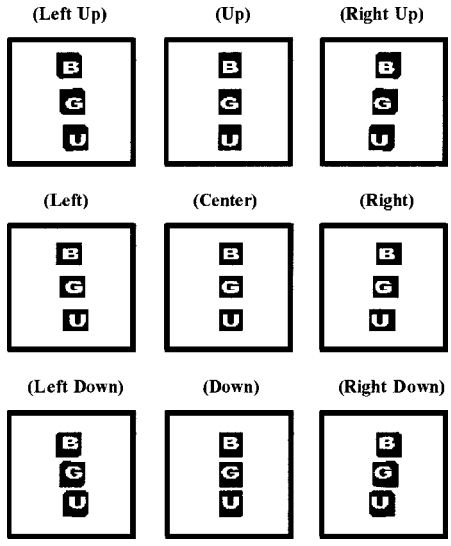

Fig. 4. Nine out of 201×201 projections of the 3D object.

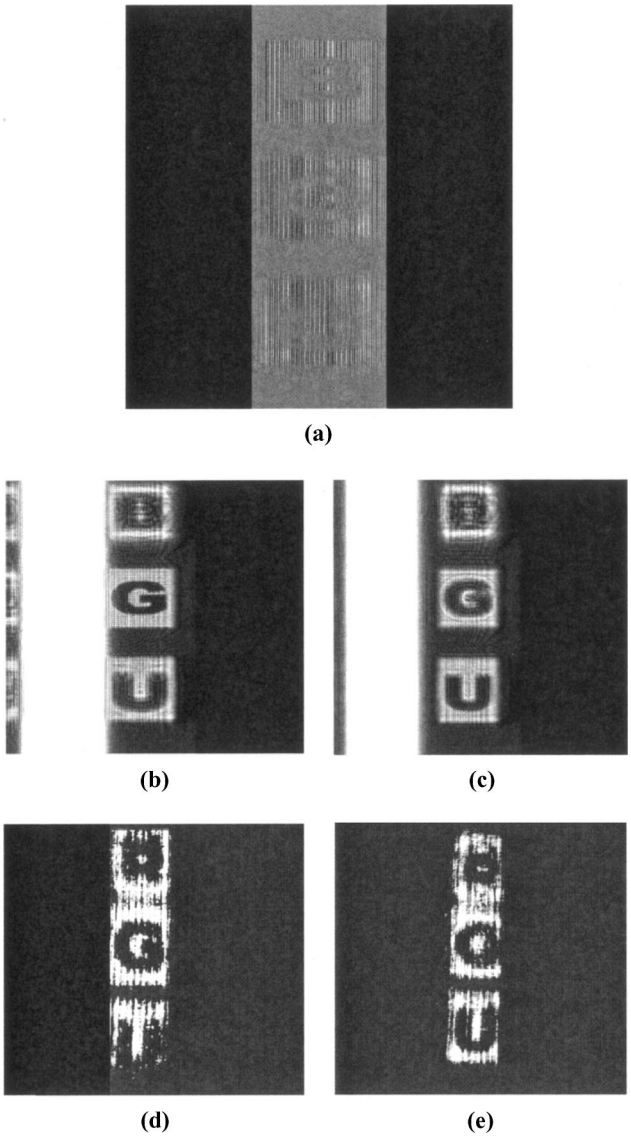

Fig. 5. (a) Enlarged portion of the intensity distribution of the image CGH. (b) and (c) The digital reconstructed images from (a). (d) and (e) The optical reconstruction. In (d) the G cube was observed at 230 mm from the lens and in (e) the U cube was observed at 270 mm from the lens.

tion 5.A, the process for generating the image CGH starts from the creation of the Fourier CGH. By computing the inverse Fourier transform of the hologram the images of the cubes are digitally reconstructed. Then, we digitally add a reference plane wave and get the desired image hologram, as shown in Fig. 5(a). The digital reconstruction from this CGH is shown in Fig. 5(b) for the G cube and in Fig. 5(c) for the U cube. The white area appearing in the center of the reconstruction is due to the influence of an intense zero-order diffraction. Although we can see that parts of the objects are in focus, other parts appear to be out of focus. This effect creates the desired illusion of an object with a considerable volume.

The experimental results of the image CGH obtained using the same previous setup are shown in Figs. 5(d) and 5(e). Also, here we used an imaging lens ($f = 400$ mm) placed between the hologram and the observer to improve visualization. The cubes G and H, shown in Figs. 5(d) and 5(e), appeared, respectively, at 230 and 270 mm from the lens, indicate the success of the 3D reconstruction. The distance between the lens and the SLM was 140 mm.

6. Conclusions

We have presented and demonstrated a process for computing three types of CGH: the Fourier–Fresnel, the Fresnel, and the image holograms. A complex function was obtained from multiple-view projections of a 3D object. This function contains the 3D information of the object and is related to the object's Fourier transform. We found that the experimental results, observed in Figs. 2, 3, and 5, are in good agreement with the theoretical and numerical simulation results that provide a strong validity of our idea. The loss of quality in the pictures of the optical reconstruction is mostly due to the poor quality of the SLM, which suffer from nonuniformity, brightness quantization, and structure of partially blocked pixels. In addition to a nonuniform illumination, the CCD records the reconstructed object in a nonideal way. All these distortion sources are accumulated for the noisy results shown in the figures. The presented techniques have a high potential in versatile holographic applications such as 3D cameras and displays.

This research was supported by Israel Science Foundation grant 119/03.

References

1. C. D. Cameron, D. A. Pain, M. Stanley, and C. W. Slinger, "Computational challenges of emerging novel true 3D holographic displays," in *Critical Technologies for the Future of Computing,* S. Bains and L. J. Irakliotis, eds., Proc. SPIE **4109,** 129–140 (2000).
2. D. Abookasis and J. Rosen, "Computer-generated holograms of three-dimensional objects synthesized from their multiple angular viewpoints," J. Opt. Soc. Am. A **20,** 1537–1545 (2003).
3. Y. Li, D. Abookasis, and J. Rosen, "Computer-generated holograms of three-dimensional realistic objects recorded without wave interference," Appl. Opt. **40,** 2864–2870 (2001).
4. Y. Sando, M. Itoh, and T. Yatagai, "Holographic three-dimensional display synthesized from three-dimensional Fourier spectra of real existing objects," Opt. Lett. **28,** 2518–2520 (2003).
5. A. B. VanderLugt, "Signal detection by complex spatial filtering," IEEE Trans. Inf. Theory **IT-10,** 139–145 (1964).
6. T. Yatagai, "Stereoscopic approach to 3-D display using computer-generated holograms," Appl. Opt. **15,** 2722–2729 (1976).
7. J.-N. Gillet and Y. Sheng, "Multiplexed computer-generated holograms with irregular-shaped polygonal apertures and discrete phase levels," J. Opt. Soc. Am. A **19,** 2403–2413 (2002).
8. A. P. Hariharan, *Optical Holography,* 2nd ed. (Cambridge U. Press, 1996), Chap. 2, pp. 19–21.
9. J. W. Goodman, *Introduction to Fourier Optics,* 2nd ed. (McGraw-Hill, 1996), Chap. 4, pp. 65–72.
10. D. Leseberg, "Computer-generated three-dimensional image holograms," Appl. Opt. **31,** 223–229 (1992).